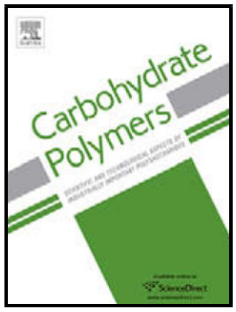

Graphene oxide enhanced ionic liquid plasticisation of chitosan/alginate bionanocomposites

Pei Chen (Methodology) (Validation)<ce:contributor-role>Formal Analysis) (Investigation), Fengwei Xie (Conceptualization) (Methodology) (Validation) (Formal analysis) (Investigation) (Resources)<ce:contributor-role>Data Curation)<ce:contributor-role>Writing - Original Draft)<ce:contributor-role>Writing - Review and Editing) (Visualization) (Supervision) (Project administration) (Funding acquisition), Fengzai Tang (Investigation)<ce:contributor-role>Writing - Original Draft), Tony McNally (Conceptualization) (Resources)<ce:contributor-role>Writing - Review and Editing) (Supervision) (Funding acquisition)

PII: S0144-8617(20)31404-1

DOI: https://doi.org/10.1016/j.carbpol.2020.117231

Reference: CARP 117231

To appear in: *Carbohydrate Polymers*

Received Date: 13 August 2020

Revised Date: 30 September 2020

Accepted Date: 9 October 2020

Please cite this article as: Chen P, Xie F, Tang F, McNally T, Graphene oxide enhanced ionic liquid plasticisation of chitosan/alginate bionanocomposites, *Carbohydrate Polymers* (2020), doi: https://doi.org/10.1016/j.carbpol.2020.117231

Graphene oxide enhanced ionic liquid plasticisation of chitosan/alginate bionanocomposites‡

Pei Chen [a,b], Fengwei Xie [b,c,*,†], Fengzai Tang [d], Tony McNally [b,**]

[a] *College of Food Science, South China Agricultural University, Guangzhou, Guangdong 510642, China*

[b] *International Institute for Nanocomposites Manufacturing (IINM), WMG, University of Warwick, Coventry CV4 7AL, United Kingdom*

[c] *School of Chemical Engineering, The University of Queensland, Brisbane, Qld 4072, Australia*

[d] *WMG, University of Warwick, Coventry CV4 7AL, United Kingdom*

[*] Corresponding author. Email addresses: d.xie.2@warwick.ac.uk, fwhsieh@gmail.com (F. Xie)

[**] Corresponding author. Email address: t.mcnally@warwick.ac.uk (T. McNally)

[†] This author leads the research.

‡ Supplementary material provided.

Highlights:

- Chitosan and chitosan/alginate plasticised by glycerol or ionic liquid (IL)
- GO/rGO improved plasticiser distribution depending on matrix and plasticiser type
- IL weakened chitosan–alginate interactions while GO counteracted this effect
- For IL-added blend, surface hydrophobicity increased with GO but reduced with rGO
- New routes in which GO or rGO interfere with biopolymer structure revealed

Abstract:

This study reports that the effect of graphene oxide (GO) or reduced GO (rGO) on the structure and properties of polyelectrolyte-complexed chitosan/alginate bionanocomposites is highly dependent on plasticiser type (glycerol or 1-ethyl-3-methylimidazolium acetate ([C_2mim][OAc])) due to the competing interactions between the components. For the glycerol-plasticised chitosan/alginate matrix, inclusion of GO/rGO enhanced the chitosan crystallinity and increased matrix ductility. While the chitosan/alginate matrix plasticised by [C_2mim][OAc] showed dramatically weakened interactions between the two biopolymers, GO was highly effective at counteracting the effect of [C_2mim][OAc] by interacting with the biopolymers and the ionic liquid ions, resulting in enhanced mechanical properties and decreased surface hydrophilicity. Compared with GO, rGO was much less effective at promoting chitosan–alginate interactions and even resulted in higher surface hydrophilicity. However, irrespective of the plasticiser type, inclusion of rGO resulted in reduced crystallinity by restricting the interactions between [C_2mim][OAc] and the biopolymers, and higher ionic conductivity.

Abbreviations: GO, graphene oxide; rGO, reduced graphene oxide; IL, ionic liquid; [C_2mim][OAc], 1-ethyl-3-methylimidazolium acetate; PEC, polyelectrolyte complexation; T_d, thermal decomposition temperature at maximum weight-loss rate; tan δ, loss tangent; T_β, peak temperature of β-transition; T_α, peak temperature of α-transition; θ_{c0s}, contact angle at 0 s; θ_{c30s}, contact angle at 60 s; θ_{c60s}, contact angle at 60 s

Keywords: Polysaccharide thermomechanical processing; Chitosan nanocomposites; Polyelectrolyte complexation; Graphene oxide; 1-Ethyl-3-methylimidazolium acetate; Glycerol

1 Introduction

Chitosan and alginate, two renewable biopolymers being biodegradable, biocompatible having inherent functionality, have great potential for use in many applications. Chitosan, a linear polysaccharide made up of β-(1,4)-linked *N*-acetyl-D-glucosamine units, is the deacetylated form of chitin, which is, in most cases, extracted from marine shell waste streams (Muxika, Etxabide, Uranga, Guerrero, & de la Caba, 2017). Chitosan has been studied widely for potential application in a wide range of sectors such as food, agriculture, pharmaceutics, biomedical treatment, cosmetics, water treatment, and textiles (Elsabee & Abdou, 2013; Muxika et al., 2017; Ravi Kumar, 2000; Rinaudo, 2006). Alginate, typically obtained from brown seaweed, is a linear, anionic polysaccharide consisting of two kinds of 1,4-linked hexuronic acid residues, namely β-D-mannuronopyranosyl (M) and α-L-guluronopyranosyl (G) residues (Yang, Xie, & He, 2011). Alginate has been extensively studied for environmental, pharmaceutical and biomedical applications (Lee & Mooney, 2012; Wang et al., 2019).

The processing of biopolymers usually requires the use of low-molecular-mass liquids as plasticisers, which can assist the disruption of the intrinsic hydrogen-bonding network in biopolymers and adjust the properties of the resulting materials by providing a plasticisation effect (Boesel, 2015; Cazón, Velazquez, Ramírez, & Vázquez, 2017; Mekonnen, Mussone, Khalil, & Bressler, 2013; Vieira, da Silva, dos Santos, & Beppu, 2011). Glycerol is the most commonly used plasticiser for biopolymers, which has been applied in the preparation of plasticised chitosan (Epure, Griffon, Pollet, & Avérous, 2011; Xie et al., 2013), alginate (Gao, Pollet, & Avérous, 2017) and starch (López et al., 2015; Shi et al., 2007) by thermomechanical processing. In recent years, ionic

liquids (ILs) have drawn huge interest for processing and plasticisation of biopolymers especially plasticised starch (Colomines, Decaen, Lourdin, & Leroy, 2016; Decaen et al., 2017; Leroy, Jacquet, Coativy, Reguerre, & Lourdin, 2012; Ren et al., 2020; Sankri et al., 2010; Xie et al., 2014; Xie et al., 2015; Zhang et al., 2016; Zhang et al., 2017). ILs that contain a strongly basic, hydrogen-bond-accepting anion (*e.g.* carboxylates or halides) are capable of disrupting the intermolecular hydrogen bonding wholly or partially in biopolymer networks (Ren et al., 2020). Meanwhile, ILs provide biopolymers with electrical conductivity (Xie et al., 2015) and open their applications in *e.g.* energy storage, biosensing and biocatalysis (Kavosi, Salimi, Hallaj, & Amani, 2014; Lu, Hu, Yao, Wang, & Li, 2006; Yamagata, Soeda, Ikebe, Yamazaki, & Ishikawa, 2013). However, there have been very few reports on IL-plasticised polysaccharides such as chitosan and alginate that are thermomechanically processed.

On the other hand, for combined or enhanced properties, hybridisation of different biopolymers or biopolymers with synthetic polymers has been commonly employed (Šimkovic, 2013; van den Broek, Knoop, Kappen, & Boeriu, 2015; Yu, Dean, & Li, 2006). For example, in food packaging, the antimicrobial efficacy of chitosan can be combined with the barrier properties of other synthetic polymers, increasing shelf life and product quality (van den Broek et al., 2015). Moreover, chitosan, as a polycation, can be complexed with negatively charged biopolymers such as alginate, carboxymethyl starch, pectin, and proteins (Mateescu, Ispas-Szabo, & Assaad, 2015), resulting in polyelectrolyte complexation (PEC). The advantages of PEC have recently been demonstrated by creating hybridised biopolymer materials with superior properties to those of either single biopolymer, such as mechanical properties (Li, Ramay, Hauch, Xiao, & Zhang, 2005; Meng, Xie,

Zhang, Wang, & Yu, 2019; Wei et al., 2019), barrier properties (Basu, Plucinski, & Catchmark, 2017), hydrolytic stability (Chen, Xie, Tang, & McNally, 2020c), and cell adhesiveness (Iwasaki et al., 2004). Deposition of chitosan together with silk fibroin or collagen on nanofibres could result in materials with excellent antimicrobial activity and cytocompatibility, promising for biomedical applications (Wu et al., 2020; Xia et al., 2019). However, there have been limited studies that have focused on the effects of plasticisers on PEC and biopolymer structure and properties. Previously, we reported that PEC between chitosan and alginate could be strongly influenced by an IL plasticiser, resulting in inferior properties (*e.g.* largely increased surface hydrophilicity) (Chen, Xie, Tang, & McNally, 2020b). How to improve the plasticisation of such hybridised biopolymer materials while maintaining their complexation and properties is a question of both scientific and practical interest.

The aim of this study is to understand the effects of graphene oxide (GO) and reduced graphene oxide (rGO) as nanofillers on the structure and properties of chitosan and chitosan/alginate blends plasticised by glycerol or 1-ethyl-3-methylimidazolium acetate ([C_2mim][OAc]). The advantages of inclusion of GO into chitosan have been demonstrated. For example, chitosan materials with GO added generally showed improved mechanical properties due to efficient load transfer between the nanofiller (GO) and chitosan matrix (Han, Yan, Chen, & Li, 2011; Yang, Tu, Li, Shang, & Tao, 2010). Furthermore, the excellent performance of chitosan/GO composites as adsorbents for metal ions (Fan, Luo, Sun, Li, & Qiu, 2013; Liu et al., 2012) and methylene blue (Fan et al., 2012) was indicated. Moreover, it was reported that biodegradable chitosan–graphene oxide (GO) composites possessed improved mechanical properties and drug delivery performance over chitosan alone (Justin & Chen, 2014). However, how the interplay between GO/rGO and plasticiser affect the

structure and properties of biopolymer PEC systems such as chitosan/alginate has not been widely explored.

In this study, the bionanocomposites were prepared by thermomechanical processing, which imparts high shear stresses enabling excellent dispersion of the nanofillers in the biopolymer matrices. Our hypothesis is that GO and rGO, containing different concentrations of oxygen-containing groups and negative charges, can be used to tailor the plasticisation of hydrophilic biopolymers in different ways. In contrast, most previous studies (Han et al., 2011; Pan, Wu, Bao, & Li, 2011; Yang et al., 2010) have focused on the surface chemistry of the nanomaterials and their direct interactions with biopolymers. Our results highlight largely unexplored routes in which GO or rGO, even in rather small loadings, interfere with blend structure and determine properties (*e.g.* mechanical properties and hydrophilicity/hydrophobicity) of such multiphasic biopolymer composites, broadening our knowledge of the potential of such biopolymer composites.

2 Materials and methods

2.1 Materials

Chitosan (poly(β-(1,4)-D-glucosamine), with a viscosity of about 200 mPa·s (*i.e.* 1% solution in 1% acetic acid at 20 °C) and a degree of deacetylation of ≥85%, was supplied by Jinan Haidebei Marine Bioengineering Co., Ltd (China). The molecular mass of this chitosan is about 250 kDa. Alginate sodium (viscosity: 200±20 mPa·s; M/G ratio: 1:1) was purchased from Shanghai Macklin Biochemical Co., Ltd (China). Graphene oxide (aqueous acid paste with 25% GO, 74% water, and 1–1.5% HCl) was acquired from Abalonyx AS (Norway). Glycerol (≥99% Analytical Grade) was supplied by Fisher Scientific UK Ltd; [C_2mim][OAc] (≥95.0%) and triacetin (99%) by Sigma-

Aldrich Company Ltd (UK); formic acid (98% w/w AR) and NaBr (pure) by Scientific Laboratory Supplies Ltd, (UK); hydrazine hydrate solution (78–82% iodometric, Honeywell Fluka) and ammonia solution (35%, AR, d = 0.88) from Fisher Scientific UK Ltd. Deionised water was used throughout the study. Reduced graphene oxide (rGO) was synthesised from GO following the method described previously (Chen, Xie, Tang, & McNally, 2020a). The characteristics of GO and rGO can be found in our previous publication (Chen et al., 2020a).

2.2 Sample preparation

Table 1 shows the formulations and codes of different samples prepared. The matrix was either chitosan alone (represented by "X") or chitosan/alginate (indicated by "Y"). The codes also signify the plasticiser used, with "G" for glycerol or "E" for [C_2mim][OAc]. The suffix "F" indicates the processed samples were films. The samples were prepared by pre-blending, thermomechanical kneading at 80 °C for 15 min, and hot-pressing at 110 °C and 160 bar for 10 min, followed by conditioning at 57% relative humidity for 3 weeks as described previously (Chen et al., 2020c). Additionally, one of the plasticisers (20 wt% based on biopolymer weight) and either GO or rGO (0.75 wt% based on biopolymer weight) were added during the pre-blending step. The samples without GO or rGO, namely XG-F, XE-F, YG-F, and YE-F, have been reported previously (Chen et al., 2020b) and are termed as controls throughout the discussion.

Table 1. Sample codes and compositions (represented as portions by weight).

Sample	Chitosan	Alginate	Plasticiser	Nanofiller	2M Formic acid solution
XG/GO-F	100	–	20, Glycerol	0.75 GO	261

XG/rGO-F	100	–	20, Glycerol	0.75, rGO	261
XE/GO-F	100	–	20, [C_2mim][OAc]	0.75, GO	261
XE/rGO-F	100		20, [C_2mim][OAc]	0.75, rGO	261
YG/GO-F	50	50	20, Glycerol	0.75, GO	261
YG/rGO-F	50	50	20, Glycerol	0.75, rGO	261
YE/GO-F	50	50	20, [C_2mim][OAc]	0.75, GO	261
YE/rGO-F	50	50	20, [C_2mim][OAc]	0.75, rGO	261

2.3 Characterisation methods

Scanning electron microscopy (SEM) imaging was performed using a Zeiss Sigma field-emission scanning electron microscope with an acceleration voltage of 6 kV. The biopolymer films were cryo-fractured using liquid nitrogen and the samples sputter-coated with gold/palladium before imaging.

Scanning transmission electron microscopy (STEM) was conducted using a Talos F200X transmission electron microscope at 200 kV to obtain both bright-field (BF) and high-angle annular dark-field (HAADF) images. Ribbons of about 60 nm thick were sectioned from epoxy-embedded sample blocks and subsequently transferred onto holey carbon films on 200-mesh copper grids. No liquids were used during sample preparation, to avoid damage to the samples.

Fourier-transform infrared (FTIR) spectra were collected using a Bruker Tensor 27 FTIR spectrometer with an attenuated total reflection (ATR) accessory acquiring 32 scans for each sample over the range 4000–500 cm^{-1} at RT.

X-ray diffraction (XRD) patterns were acquired using a Panalytical Empyrean X-ray diffractometer at 40 kV and 40 mA with a Co target (Kα = 1.790307 Å) and a beam slit of 10 mm.

The samples were scanned over an angular range (2θ) of 6–40° with a step size of 0.0263° and a step rate of 2.16 s/step. Crystal lattice spacing (*d*-spacing) is calculated according to Bragg's Law:

$$d = \frac{n\lambda}{2sin\theta} \qquad (1)$$

where θ is the angle of incidence, λ is the wavelength of the incident light, n is an integer.

Thermo-gravimetric analysis (TGA) was undertaken using a Mettler Toledo TGA apparatus over a temperature range of 30–700 °C at 10 K/min under nitrogen.

Dynamic mechanical thermal analysis (DMTA) was performed using a Tritec 2000 DMA (Triton Technology Ltd, UK) in dual cantilever mode with a sample length of 5 mm at a displacement of 0.01 mm. Temperature scans were performed from −100 °C to 180 °C at 2 °K/min and 1 Hz.

Tensile testing was performed using an Instron 3367 universal testing machine with a 1kN load cell at a crosshead speed of 3 mm/min. As the specimens were in the form of thin sheets, specimen extension was measured by grip separation as suggested by ASTM Standard D882. At least seven replicates were used for each sample.

Contact angle (θ_c) data was obtained from sessile tests at RT based on Young–Laplace using an Attension Theta Lite instrument (Biolin Scientific, UK). As θ_c kept changing after a drop of water was placed onto the sample surface, θ_c values at 0 s, 30 s, and 60 s (denoted as θ_{c0s}, θ_{c30s}, and θ_{c60s} respectively) were recorded.

Electrical impedance spectroscopy (EIS) was performed using a Princeton Applied Research PARSTAT MC (PMC) multi-channel potentiostat (Ametek Scientific Instruments, USA) with a PMC-2000 card and a two-point probe. The two surfaces of samples were painted with carbon

conductive grease (No.8481, MG Chemicals, Canada) in designated areas (24 × 24 mm). Each sample was measured in triplicate. The real (Z') and imaginary (Z'') parts of impedance were acquired within a frequency (f) range of 1–10^6 Hz. The AC conductivity (admittance) (σ), the real part of relative permittivity (ε'_r), and the imaginary part of electric modulus (M'') were calculated using the following equations (Bhatt, Bhat, Santosh, & Tai, 2011; Bowen Chris, Buschhorn, & Adamaki, 2014; Osman, Ibrahim, & Arof, 2001):

$$\sigma = \frac{Z\prime}{Z\prime^2 + Z\prime\prime^2} \cdot \frac{t}{A} \quad (2)$$

$$\varepsilon'_r = \frac{-Z\prime\prime}{Z\prime^2 + Z\prime\prime^2} \cdot \frac{t}{\omega A \varepsilon_0} \quad (3)$$

$$M'' = \frac{\varepsilon\prime\prime}{\varepsilon\prime^2 + \varepsilon\prime\prime^2} \quad (4)$$

where, ω is the angular frequency (= $2\pi f$), ε_0 is the permittivity of free space (≈ 8.854 ×10^{-12} F·m^{-1}), A is the tested area of the sample (m^2), and t is the sample thickness (m).

The bulk resistance (R_b) was determined from the Nyquist plots of impedance (Z'' *vs.* Z') from the points where the semicircle and the straight line meet. Then, the conductivity (σ_{dc}) can be calculated using equation (5) (Fadzallah, Majid, Careem, & Arof, 2014; Osman et al., 2001):

$$\sigma_{dc} = \frac{t}{R_b \cdot A} \quad (5)$$

3 Results and Discussion

3.1 Morphology

Figure S1 shows SEM images of cryo-fractured surfaces of the different bionanocomposite films. For the X-series of composites, the morphology was not altered on inclusion of either GO or rGO. In contrast, for the Y-matrix plasticised by either glycerol or [C_2mim][OAc], inclusion of either GO or rGO clearly promoted phase distribution and yielded more cohesive surfaces. In particular,

our previous study (Chen et al., 2020b) indicated that [C_2mim][OAc] could significantly interfere with PEC between chitosan and alginate, since there could be interactions of the $[OAc]^-$ anion with the hydroxyl and amine groups of chitosan and of the $[C_2mim]^+$ cation with the carboxylate groups of alginate. However, here, addition of GO at only 0.75 wt% loading apparently disrupted the effect of [C_2mim][OAc] on phase structure.

The morphology of the different bionanocomposites was further studied using STEM, as shown in **Figure 1**. For the X-series of composites, minor traces of GO/rGO agglomerations can be seen. Given this observation, it is considered that the GO/rGO nanosheets were largely exfoliated and dispersed in the matrices either as few-layer nanoplatelets, which lost contrast under STEM and difficult to image. GO nanosheets are generally negatively charged resulting from the ionisation of the oxygen-containing groups (*e.g.* ─COOH and ─OH). Therefore, dispersion could also be promoted by hydrogen-bonding and electrostatic interactions between the chitosan polycation and the negatively charged GO nanosheets (Yang et al., 2010). Excellent dispersion of GO in chitosan materials has also been noted in previous studies (Han et al., 2011; Pan et al., 2011; Yang et al., 2010). In the Y-series of composites, large GO/rGO agglomerations are more frequently observed although they are small in number. It is likely that PEC between chitosan and alginate competed with the interactions between GO/rGO and chitosan to some extent.

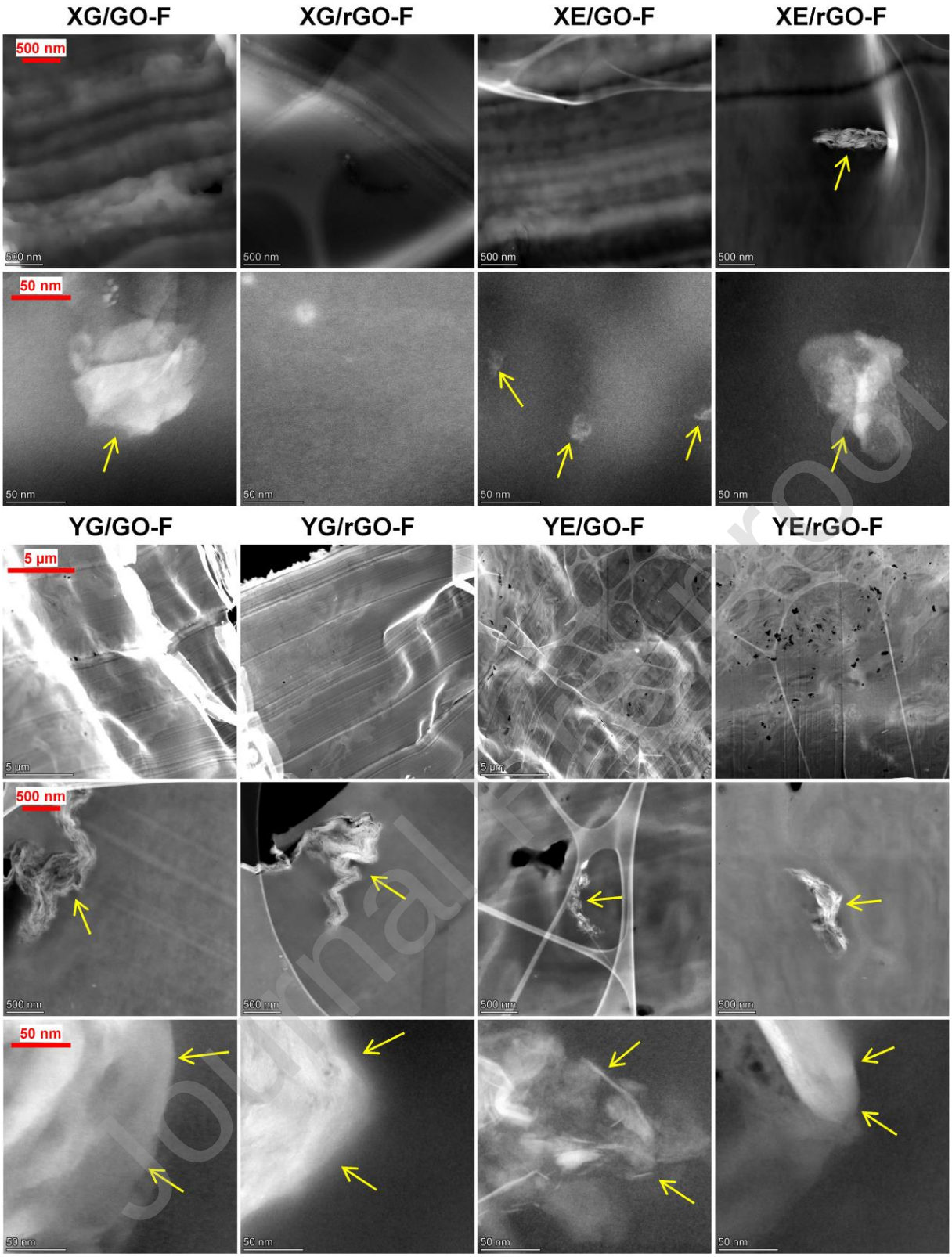

Figure 1. Scanning transmission electron microscopy high-angle annular dark-field (STEM-HAADF) images of the different bionanocomposite films. The yellow arrows indicate GO/rGO agglomerations (not fully exfoliated).

For the Y-series of samples, a “new structure” was also observed normally at the edges of the areas imaged (where the material has no or much less interaction with the electron beam) (**Figure S2**), which is highly interesting. Given this, the energy from the electron beam could possibly facilitate coordination between alginate and $[C_2mim]^+$ and the packing of polysaccharide chains to form crystals, in an analogy to the formation of junction zones by alginate with Ca^{2+} (Li, Fang, Vreeker, Appelqvist, & Mendes, 2007; Morris, Rees, Thom, & Boyd, 1978; Sikorski, Mo, Skjåk-Bræk, & Stokke, 2007). This phenomenon was further investigated.

3.2 Fourier-transform infrared (FTIR) spectroscopy

Figure 2 shows the FTIR spectra for the different bionanocomposites. The X-series of composites displayed FTIR patterns very similar to those for XG-F and XE-F (Chen et al., 2020b), indicating inclusion of GO or rGO did not significantly alter the molecular interactions in the plasticised chitosan matrices. Compared with the X-series, the Y-series had blue shifts of the peaks originally at 1570 cm^{-1} and 1024 cm^{-1}. The peak at 1570 cm^{-1} is assigned to the N─H bending vibration from amine and amide II (Lawrie et al., 2007) and the one at 1024 cm^{-1} is attributed to the skeletal vibration of C─O stretching (Lawrie et al., 2007; Papageorgiou et al., 2010). Thus, PEC should have involved amine and amide groups and affected the saccharide ring structure.

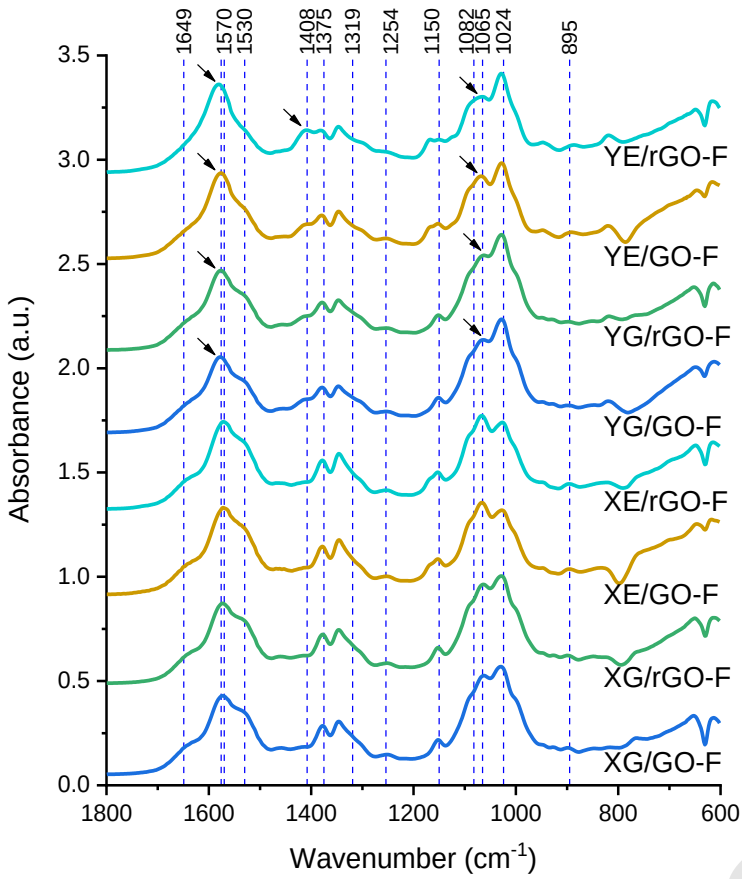

Figure 2. Fourier-transform infrared (FTIR) spectra for the different bionanocomposite films. The reference lines indicate the characteristic peak for X-F / XG-F, except for 1408 cm^{-1} and 1082 cm^{-1}, which are for original alginate (Chen et al., 2020b). The arrows indicate shifts in peak position or changes in peak intensity.

The FTIR patterns for YG/GO-F and YG/rGO-F are nearly identical to that for YG-F (Chen et al., 2020b), indicating inclusion of GO or rGO had a negligible effect on the molecular interactions of the chitosan/alginate matrix plasticised by glycerol. For YE-F (Chen et al., 2020b), there was a greater deviation in the position of the peak originally at 1570 cm^{-1} (N─H bending of chitosan), the peak at 1408 cm^{-1} (symmetric COO^- stretching of alginate (Lawrie et al., 2007; Papageorgiou et al., 2010)) became more intense, and the peak at 1065 cm^{-1} (asymmetric C─O─C stretching in the glycosidic linkage of chitosan (Chen, Mo, He, & Wang, 2008; Lawrie et al., 2007; Pawlak & Mucha,

2003) and alginate (Lawrie et al., 2007; Papageorgiou et al., 2010)) became less intense, which is caused by the weakened PEC and hydrogen bonding between chitosan and alginate with the presence of [C_2mim][OAc]. With inclusion of GO, these changes induced by the IL were apparently suppressed since YE/GO-F showed an FTIR pattern similar to that for YG-F, YG/GO-F and YG/rGO-F. This is caused by the interactions of GO (negatively charged) with the IL (especially the $[C_2mim]^+$ cation) and with the chitosan cation. rGO was also seen to counteract the effect of the IL on biopolymer molecular interactions, but to a much lesser extent than GO.

3.3 X-ray diffraction (XRD) analysis

Figure 3 shows the XRD curves for the different bionanocomposite films. All the X-series of composites displayed similar diffractograms to those for XG-F and XE-F (Chen et al., 2020b). For all these samples, there were three major peaks at 2θ of about 13.5° ((020) reflection, *d*-spacing = 0.76 nm), 21.7° ((100) reflection, 0.48 nm), and 27.2° ((110) reflection, 0.38 nm), attributable to the crystal lattice of chitosan (Kittur, Vishu Kumar, & Tharanathan, 2003). As the XRD pattern of the processed chitosan was completely different from that of original chitosan, the crystalline structure in the composites should be predominantly due to re-crystallisation (Chen et al., 2020b). Inclusion of GO/rGO did not change the recrystallised structure of plasticised chitosan.

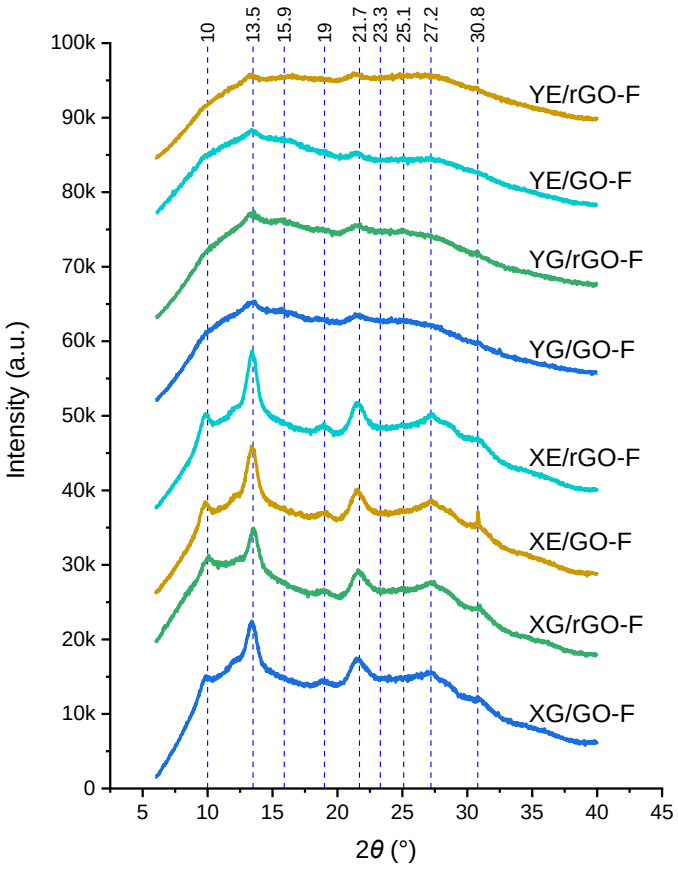

Figure 3. X-ray diffractograms for the different bionanocomposite films. The reference lines indicate the characteristic peaks for X-F / XG-F (Chen et al., 2020b).

All the Y-series of composites displayed a low degree of crystallinity as YG-F and YE-F did (Chen et al., 2020b). A predominantly amorphous structure should result from PEC between chitosan and alginate. Compared with YG-F, YG/GO-F and YG/rGO-F had slightly stronger peak intensities especially at 13.5° and 21.7°, suggesting that inclusion of GO or rGO increased the crystallinity of chitosan plasticised by glycerol. However, YE/rGO-F showed even weaker peak intensities than YE-F. In this case, while [C_2mim][OAc] had an apparent effect and enhanced polysaccharide re-crystallisation (Chen et al., 2020b), rGO may have restricted the interaction between the IL and the

polysaccharides. A similar result was also observed for a chitosan/carboxymethyl cellulose/rGO composite plasticised by [C_2mim][OAc] (Chen, Xie, Tang, & McNally, 2020d).

3.4 Thermogravimetric analysis (TGA)

Figure 4 shows the curves of derivative weight as a function of temperature for the different bionanocomposites. For the chitosan matrix plasticised by either glycerol or [C_2mim][OAc], the peak temperature of the major weight loss (T_d, at the maximum weight-loss rate) was not affected by addition of GO. Specifically, XG-F (Chen et al., 2020b) and XG/GO-F had the same T_d value of 283 °C; and both XE-F (Chen et al., 2020b) and XE/GO-F had T_d = 264 °C. Nonetheless, inclusion of rGO slightly reduced T_d (277 °C and 261 °C for XG/rGO-F and XE/rGO-F, respectively). In this regard, rGO may have disrupted the hydrogen-bonded network to some extent in the plasticised chitosan systems.

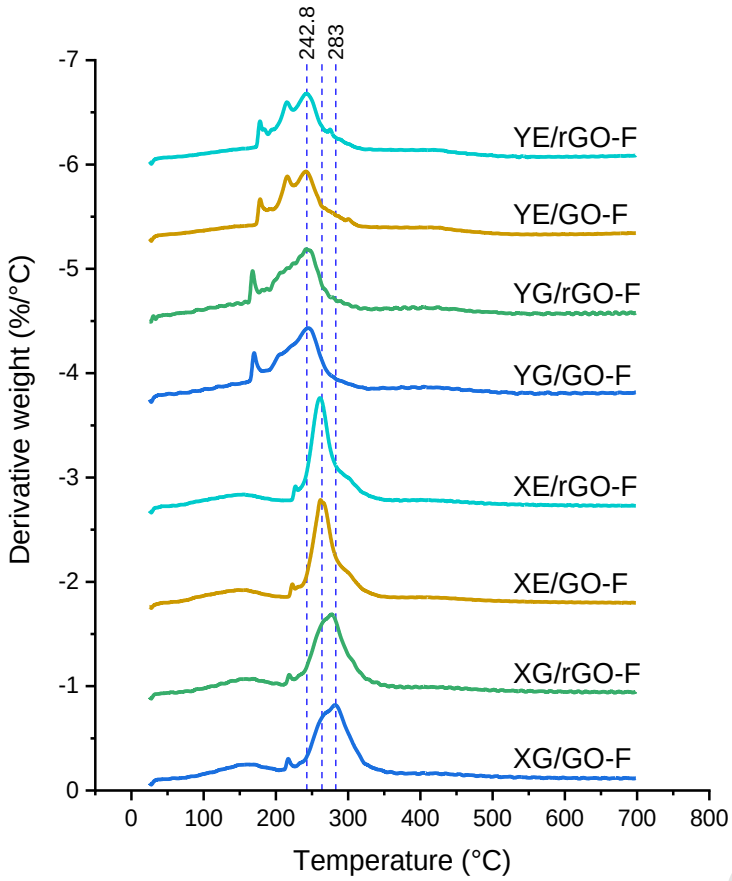

Figure 4. Derivative weight *vs.* temperature curves measured by thermogravimetric analysis (TGA) for the different bionanocomposite films. The reference lines indicate the major peak temperatures of XG-F (283 °C), XE-F (264 °C), and YG-F / YE-F (243 °C), respectively (Chen et al., 2020b).

The Y-series of composites had T_d unchanged relative to those for YG-F and YE-F (243 °C) (Chen et al., 2020b). For YG-F, YG/GO-F, and YG/rGO-F, the derivative-weight peak of alginate (peak temperature at 206 °C) should be overlapped with that of chitosan and was just about visible. Considering the T_d values for unprocessed chitosan and alginate are 289 °C and 232 °C respectively (Chen et al., 2020b), complexation between chitosan and alginate dramatically resulted in decreased thermal stability of both polysaccharides. In contrast for the Y-series plasticised by glycerol, for YE-F (Chen et al., 2020b), YE/GO-F, and YE/rGO-F, the alginate peak became more prominent and

appeared at a higher temperature (216 °C), associated with the weakened interactions between the two biopolymers caused by [C_2mim][OAc], as discussed above.

3.5 Dynamic mechanical thermal analysis (DMTA)

Figure 5 shows the loss tangent (tan δ) plots as a function of temperature, which show two transitions for all the bionanocomposites. The weak, sub-zero transition is associated with the chitosan side-chain motion or lateral groups interacting with small molecules such as water and plasticisers (*i.e.* a β-relaxation); and the more prominent transition at higher temperature is attributed to the α-transition (glass transition) of chitosan (Quijada-Garrido, Laterza, Mazón-Arechederra, & Barrales-Rienda, 2006; Quijada-Garrido, Iglesias-González, Mazón-Arechederra, & Barrales-Rienda, 2007).

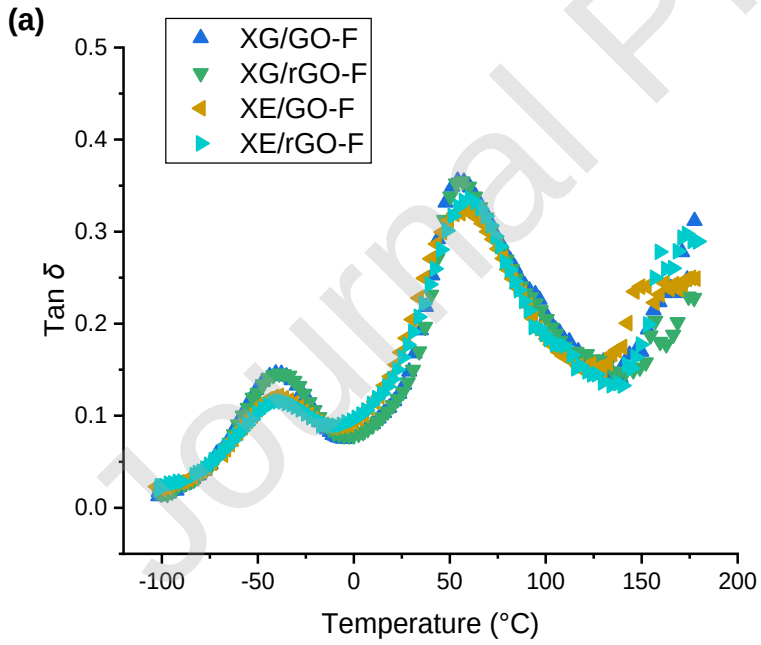

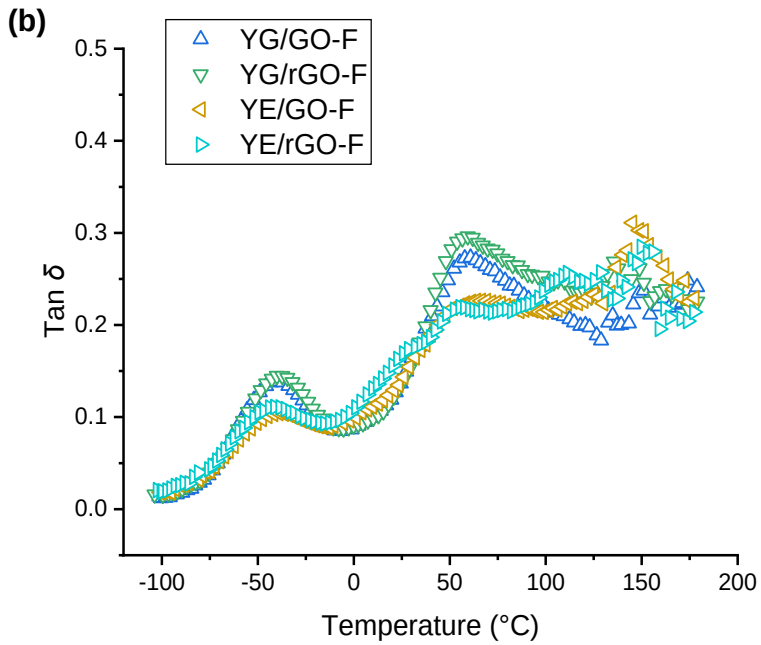

Figure 5. Loss tangent (tan δ) as a function of temperature measured by dynamic mechanical thermal analysis (DMTA) for the different bionanocomposite films: a) chitosan matrix; b) chitosan/alginate matrix.

Compared with XG-F and XE-F (Chen et al., 2020b), the bionanocomposites with either GO or rGO did not show apparent variations in the β-relaxation or α-transition. Besides, YG/GO-F and YG/rGO-F displayed almost the same tan δ profile as that for YG-F (Chen et al., 2020b), suggesting GO or rGO also did not vary the transition temperatures of the chitosan/alginate matrix plasticised by glycerol. However, while YE-F seemingly had two α-transitions with peak temperatures at 49 °C and 111 °C, respectively (Chen et al., 2020b), this profile became less apparent for YE/GO-F, which showed a single transition peaked at about 65 °C. This is a result of the reduction in phase separation between chitosan and alginate caused by [C_2mim][OAc] and inclusion of GO. Nonetheless, YE/rGO-F displayed a tan δ profile very close to that for YE-F, suggesting rGO was not as effective as GO at

disrupting the weakened interactions between chitosan and alginate caused by the IL. In this sense, the DMTA results here are in agreement with the FTIR analysis.

3.6 Mechanical properties

Representative stress–strain profiles from tensile testing (**Figure S3**) of the different bionanocomposite films indicates they were hard and tough. From these curves, the Young's modulus (E), tensile strength (σ_t), and elongation at break (ε_b) were calculated and plotted in **Figure 6** (a), (b), and (c), respectively. Inclusion of GO or rGO has a negligible effect on the mechanical properties of the X-matrix plasticised by glycerol as the E, σ_t, and ε_b values for XG/GO-F and XG/rGO-F were similar to those for XG-F (Chen et al., 2020b). However, for the X-matrix plasticised by [C_2mim][OAc], inclusion of both GO and rGO significantly reduced E and increased ε_b, with rGO being more effective. Specifically, compared with XE-F (E = 530±43 MPa and ε_b = 186.8±17.0%) (Chen et al., 2020b), XE/GO-F had E = 251±49 MPa and ε_b = 228.8±25.4% and XE/rGO-F had E = 142±46 MPa and ε_b = 287.9±21.7%, suggesting higher ductility. In this regard, the inclusion of GO or rGO appears to have increased the plasticisation effect of [C_2mim][OAc]. Regarding this phenomenon, we speculate that the excellent dispersion of GO or rGO nanoplatelets decreased the localisation of the IL (as the plasticiser distribution in the polysaccharide may not be fully uniform originally) and improved its distribution in the chitosan, thus weakening chitosan chain interactions in amorphous regions.

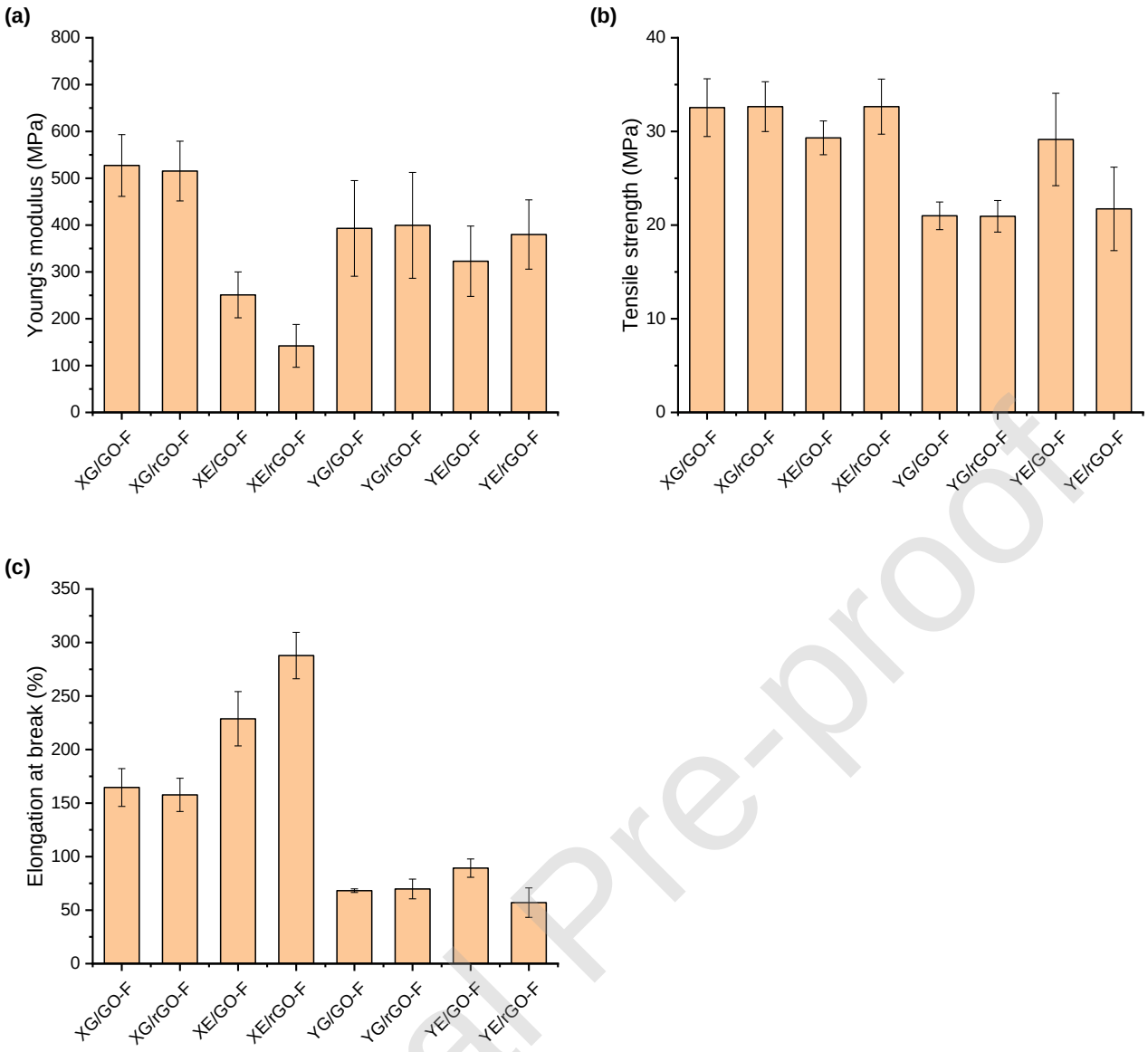

Figure 6. Tensile mechanical properties a) Young's modulus, b) tensile strength and c) elongation at break of the different bionanocomposite films. Error bars represent standard deviations.

Compared with YG-F (E = 587±105 MPa and ε_b = 51.1±4.9%) (Chen et al., 2020b), both YG/GO-F and YG/rGO-F displayed a decrease in E (393±102 MPa and 399±113 MPa, respectively) and an increase in ε_b (68.2±1.7% and 69.8±9.2%, respectively). This suggests inclusion of GO or rGO may have improved the distribution of glycerol in the Y-matrix (especially in the alginate phase) and reduced polysaccharide chain interactions in amorphous regions and, thus, resulted in

increased ductility. On the other hand, compared with YE-F (E = 456±57 MPa, σ_t = 23.3±4.4 MPa, and ε_b = 64.5±12.0%), YE/rGO-F had similar mechanical properties, whereas YE/GO-F had lower E (323±75 MPa) but higher σ_t (29.1±4.9) and ε_b (89.3±8.6%). As discussed above, [C_2mim][OAc] disturbs PEC between chitosan and alginate whereas GO counteracts the effect of the IL, reflected in the enhancement in strength and ductility of YE/GO-F.

Despite these effects of GO or rGO on the tensile properties, **Figure S4** shows that the Shore D hardness was not apparently influenced by their inclusion regardless of the matrix. The Shore D hardness was mainly influenced by the plasticiser especially, for the X-matrix.

3.7 Contact angle

Figure 7 shows the θ_{c0s}, θ_{c30s}, and θ_{c60s} values for the different bionanocomposite films, as contact angle kept changing during the sessile measurement. Our previous study (Chen et al., 2020b) indicated that XG-F had θ_{c0s} = 102±6°, θ_{c30s} = 81±4°, and θ_{c60s} = 73±3° and XE-F had θ_{c0s} = 95±3°, θ_{c30s} = 74±4°, and θ_{c60s} = 70±4°. For the X-matrix regardless of plasticiser type, inclusion of GO or rGO did not cause notable changes in contact angle, *i.e.* all have similar surface hydrophilicity. In this regard, the surface hydrophilicity was predominantly determined by the polarities of chitosan and plasticiser groups on the film surface, which were not varied by GO or rGO.

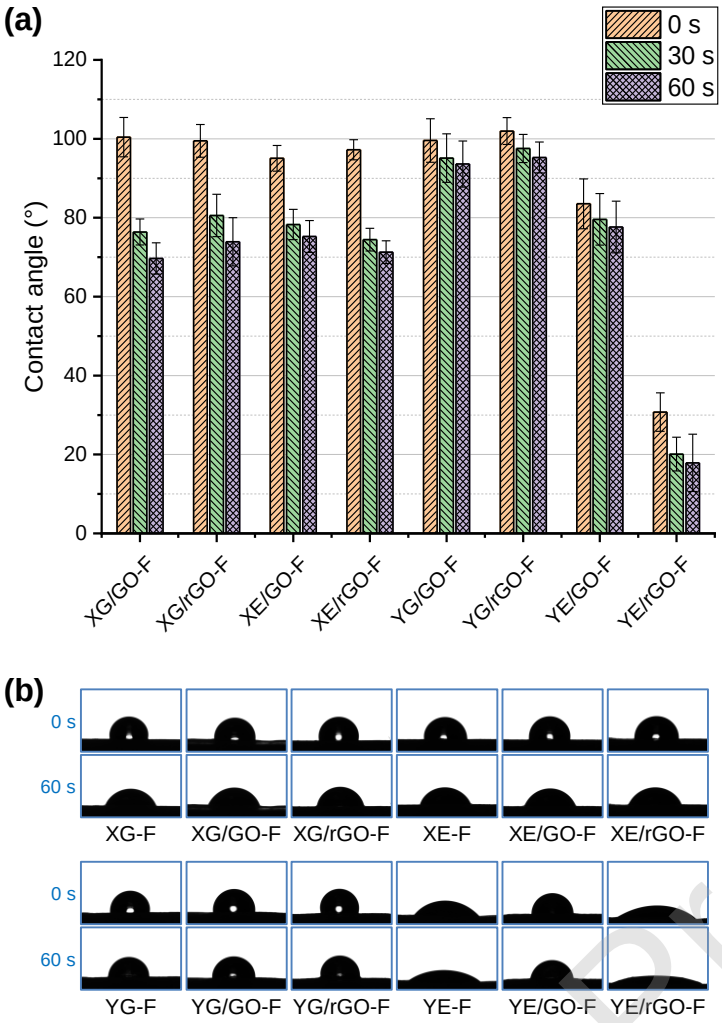

Figure 7. Contact angle values at 0 s, 30 s, and 60 s for the different bionanocomposite films. Error bars represent standard deviations. XG-F, XE-F, YG-F, and YE-F were measured in our previous study (Chen et al., 2020d).

Compared with YG-F (θ_{c0s} = 98±6°, θ_{c30s} = 95±6°, and θ_{c60s} = 93±6°), YG/GO-F and YG/rGO-F did not show apparent changes in contact angle. However, for the [C_2mim][OAc]-plasticised Y-matrix, the surface hydrophilicity was remarkably varied by inclusion of GO or rGO even at 0.75 wt% loading, which is surprising. Specifically, while YE-F had θ_{c0s} = 48±5°, θ_{c30s} = 36±5°, and θ_{c60s} = 33±5°, these values were dramatically increased to 84±6°, 80±7°, and 78±7° respectively for

YE/GO-F whereas decreased to 31±5°, 20±4°, and 18±7° respectively for YE/rGO-F. The reduced surface hydrophilicity for YE/GO-F can again be, ascribed to the less-interfered PEC between the two polysaccharides by [C_2mim][OAc] with the presence of GO, as discussed above. In addition, the interaction of GO with the IL could also limit the binding of the IL with water, also contributing to decreasing surface wettability. In comparison, rGO was much less effective than GO to counteract the effect of the IL and, thus, the interactions between chitosan and alginate were still weak. Meanwhile, rGO could dissociate some IL ions and/or the polysaccharide hydrophilic groups from interactions, which could then readily bind with water. In this regard, YE/rGO-F even had a greater surface wettability than YE-F.

3.8 Electrochemical impedance spectroscopy (EIS)

Figure 8 (a) shows the Nyquist plots of impedance (Z'' *vs.* Z') for the different bionanocomposite films. Based on these plots, the R_b and σ_{dc} values calculated (Bonanos, Steele, & Butler, 2005) are listed in **Table S1**. Compared with XG-F (σ_{dc} = (3.93±0.70)×10^{-5} S·cm^{-1}) (Chen et al., 2020b), only XG/rGO-F showed an apparent increase in σ_{dc}, which should be associated with the intrinsic conductivity of rGO. XE/GO-F and XE/rGO-F had similar σ_{dc} values to that for XE-F ((6.85±0.78)×10^{-5} S·cm^{-1}). Given this result, the conductivity of the X-samples plasticised by [C_2mim][OAc] could be mainly determined by the IL as a salt (Wang, Chi, & Mu, 2014). YG/GO-F and YG/rGO-F had σ_{dc} about twice that of YG-F ((2.80±0.31)×10^{4} S·cm^{-1}) (Chen et al., 2020b), suggesting inclusion of the 2D nanofillers contributed to the electrical charges (ions and dipoles) in the polysaccharide composite system. Compared with YE-F (σ_{dc} = (2.74±0.20)×10^{-5} S·cm^{-1}) (Chen et al., 2020b), YE/GO-F displayed similar σ_{dc} whereas YE/rGO-F had a higher value

($(6.54\pm0.82)\times10^{-5}$ S·cm^{-1}). Although GO could disrupt the interactions between the IL ions and the respective biopolymers, its interactions with the IL ions and the polysaccharides could limit the mobility of the electrical charges. The increased σ_{dc} value of YE/rGO-F could be derived from the conductivity of rGO, as well as the greater availability of IL ions and/or the polysaccharide hydrophilic groups, as discussed above.

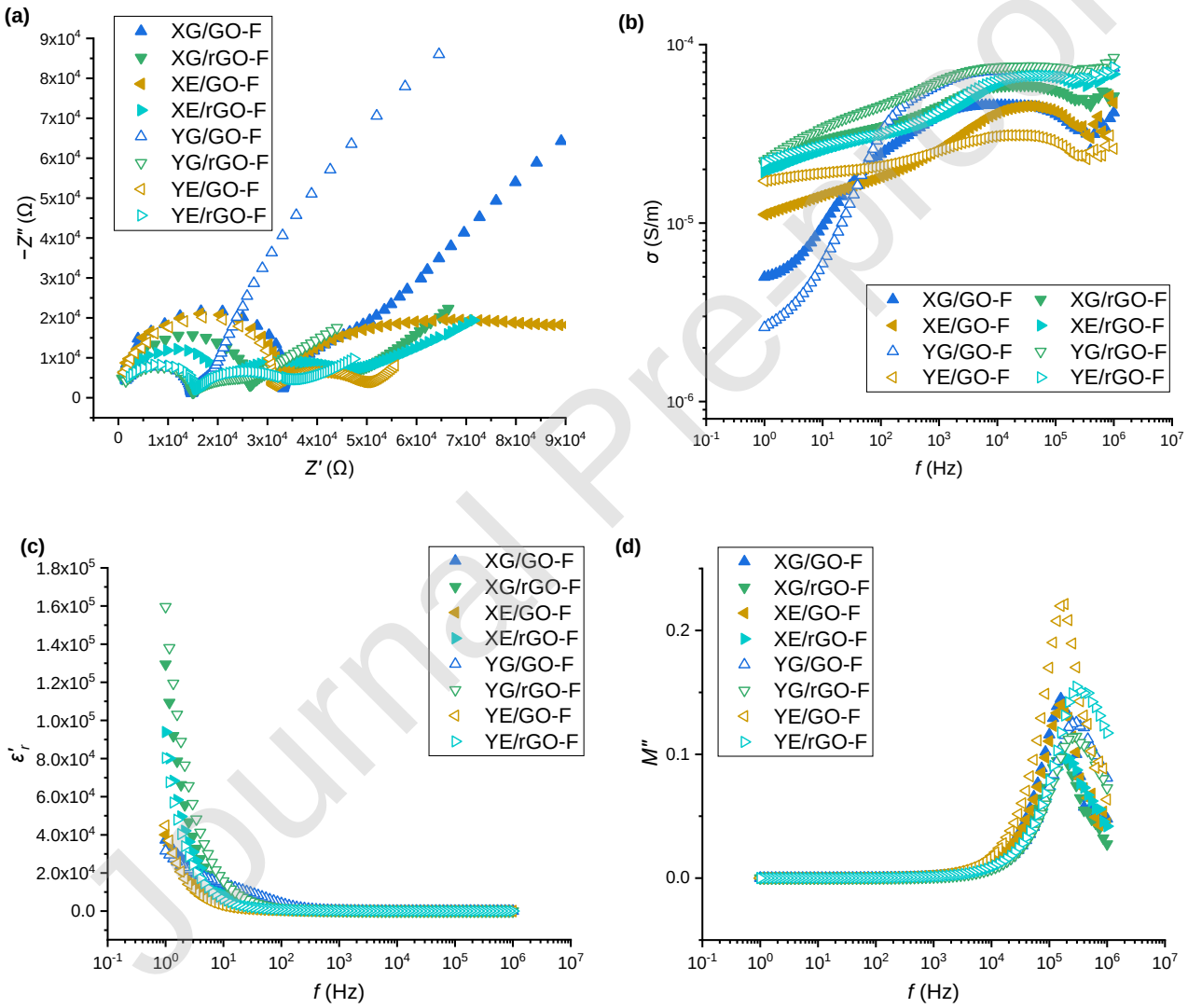

Figure 8. Electrical impedance spectroscopy (EIS) results for the different bionanocomposite films: a) Nyquist plot of impedance; b) AC conductivity (σ); c) real relative permittivity (ε'_r); and d) imaginary electric modulus (M'').

Figure 8 (b) shows that for all the bionanocomposite films, σ increased with f, typical of an insulating material (dielectric). The four samples containing rGO displayed higher σ especially at low f (< 250 Hz) and less dependency of σ on f than other samples and the controls (XG-F, XE-F, YG-F and YE-F) (Chen et al., 2020b). In this regard, rGO contributed to the overall conductivity of the materials.

Figure 8 (c) shows that decreasing f led to an abrupt increase in ε'_r, which could be ascribed to electrode polarisation and space charge effects (dipole moment) (Khiar, Puteh, & Arof, 2006; Navaratnam et al., 2015). Compared with the controls (Chen et al., 2020b), the bionanocomposites with GO had higher ε'_r at low f (<50 Hz). And, inclusion of rGO had an even greater effect on ε'_r at low f. In this regard, rGO could be more effective than GO at facilitating the accumulation of mobile ions. Moreover, the bionanocomposites displayed impressively high ε'_r at 1 kHz (over 150) except for YE/GO-F (**Table S1**). For YE/GO-F, the strong interaction of GO with the IL ions and the polysaccharide polar groups could restrict the dipole moment.

Figure 8 (d) shows that for all the bionanocomposites, there was a well-defined peak in M'' at high f, indicating relaxation processes with distributed relaxation times (*i.e.* viscoelastic relaxation, or dipolar relaxation) (Fadzallah et al., 2014). Compared to XG-F whose M'' peak position was at about 1.4×10^5 Hz (Chen et al., 2020b), both XG/GO-F and XG/rGO-F had the peak moved to 1.7×10^5 Hz, indicating reduced relaxation time. In this regard, inclusion of GO or rGO increased the mobility of ions and associated dipoles. XE-F, XE/GO-F and XE/rGO-F had similar peak positions at about $1.7–1.8\times10^5$ Hz, suggesting no apparent effect of the nanofillers on the relaxation time for

the X-matrix plasticised by [C_2mim][OAc]. In other words, in these three samples, the mobility of ions and dipoles could be mainly determined by the IL. On the other hand, while the peak position for YG-F was about 1.7×10^5 Hz, YG/GO-F and YG/rGO-F displayed a peak position at about 2.9–3.2×10^5 Hz. Compared with YE-F peak position at about 1.5×10^5 Hz, YE/GO-F and YE/rGO showed peak positions at about 1.7×10^5 Hz and 2.9×10^5 Hz, respectively. These results indicate increased mobility of ions and dipoles by inclusion of GO or rGO to the Y-matrix. In particular, the short relaxation time for YE/rGO-F corresponds to the disrupted interactions between the IL ions and polysaccharides, as discussed above.

4 Conclusions

This study shows that for the chitosan/alginate matrix, inclusion of GO or rGO affected composite structure and properties via different mechanisms. For the glycerol-plasticised Y-matrix, inclusion of GO or rGO increased the crystallinity and ductility of the chitosan, probably by assisting the distribution of glycerol in the Y-matrix (especially in the alginate phase). While [C_2mim][OAc] could dramatically weaken PEC and hydrogen bonding between chitosan and alginate, FTIR and DMTA results suggest that GO was capable of counteracting the effect of the IL by interacting with the IL and the polysaccharides, leading to remarkably increased matrix strength and decreased surface hydrophilicity. In comparison, rGO was far less effective at promoting chitosan–alginate interactions. However, rGO could still release some IL ions and/or the polysaccharide hydrophilic groups from participating in interactions, reflected by lower crystallinity and even higher surface hydrophilicity for YE/rGO-F.

For the X-matrix plasticised by glycerol and [C_2mim][OAc], the effect of GO or rGO on the structure and properties was minor, most likely due to the dominant interactions between plasticiser and chitosan. However, for the [C_2mim][OAc]-plasticised X-matrix, inclusion of GO or rGO increased ductility, with rGO being more effective, behaviour attributed to the GOs being capable of improving the distribution of this plasticiser in the chitosan matrix.

Thus, this work has shown the different ways in which these 2D carbon materials influence the structure and properties of polysaccharides and, in particular, the efficacy of GO to overcome the negative effects of the IL cation on PEC in polysaccharide materials. This information could be insightful for the design of various biopolymer composite systems where multiple interactions among components can be manipulated so as to tailor properties.

Conflicts of Interests

Declarations of interest: none

5 CRediT author statement:

Pei Chen: Methodology, Validation, Formal Analysis, Investigation. **Fengwei Xie:** Conceptualization, Methodology, Validation, Formal analysis, Investigation, Resources, Data Curation, Writing - Original Draft, Writing - Review & Editing, Visualization, Supervision, Project administration, Funding acquisition. **Fengzai Tang:** Investigation, Writing - Original Draft. **Tony**

McNally: Conceptualization, Resources, Writing - Review & Editing, Supervision, Funding acquisition.

Acknowledgements

The authors acknowledge funding from the European Union's Horizon 2020 research and innovation programme under the Marie Skłodowska-Curie grant agreement No. 798225. P. Chen acknowledges the financial support from the China Scholarship Council (CSC) for her visiting position and thanks IINM, WMG, University of Warwick, UK for hosting her research visit. F. Xie also acknowledges support from the Guangxi Key Laboratory for Polysaccharide Materials and Modification, Guangxi University for Nationalities, China (grant No. GXPSMM18ZD-02).

References

Basu, S., Plucinski, A., & Catchmark, J. M. (2017). Sustainable barrier materials based on polysaccharide polyelectrolyte complexes. *Green Chemistry*, *19*(17), 4080-4092.

Bhatt, A. S., Bhat, D. K., Santosh, M. S., & Tai, C.-w. (2011). Chitosan/NiO nanocomposites: a potential new dielectric material. *Journal of Materials Chemistry*, *21*(35), 13490-13497.

Boesel, L. F. (2015). Effect of plasticizers on the barrier and mechanical properties of biomimetic composites of chitosan and clay. *Carbohydrate Polymers*, *115*(0), 356-363.

Bonanos, N., Steele, B. C. H., & Butler, E. P. (2005). Applications of Impedance Spectroscopy. In E. Barsoukov, & J. R. Macdonald (Eds.), *Impedance Spectroscopy* (pp. 205-537). Hoboken, NJ, USA: John Wiley & Sons, Inc.

Bowen Chris, R., Buschhorn, S., & Adamaki, V. (2014). Manufacture and characterization of conductor-insulator composites based on carbon nanotubes and thermally reduced graphene oxide. *Pure and Applied Chemistry, 86*(5), 765-774.

Cazón, P., Velazquez, G., Ramírez, J. A., & Vázquez, M. (2017). Polysaccharide-based films and coatings for food packaging: A review. *Food Hydrocolloids, 68*, 136-148.

Chen, P., Xie, F., Tang, F., & McNally, T. (2020a). Structure and properties of thermomechanically processed chitosan/carboxymethyl cellulose/graphene oxide polyelectrolyte complexed bionanocomposites. *International Journal of Biological Macromolecules, 158*, 420-429.

Chen, P., Xie, F., Tang, F., & McNally, T. (2020b). Unexpected Plasticization Effects on the Structure and Properties of Polyelectrolyte Complexed Chitosan/Alginate Materials. *ACS Applied Polymer Materials, 2*(7), 2957-2966.

Chen, P., Xie, F., Tang, F., & McNally, T. (2020c). Thermomechanical-induced polyelectrolyte complexation between chitosan and carboxymethyl cellulose enabling unexpected hydrolytic stability. *Composites Science and Technology, 189*, 108031.

Chen, P., Xie, F., Tang, F., & McNally, T. (2020d). Ionic Liquid (1-Ethyl-3-methylimidazolium Acetate) Plasticization of Chitosan-Based Bionanocomposites. *ACS Omega, 5*(30), 19070-19081.

Chen, Z., Mo, X., He, C., & Wang, H. (2008). Intermolecular interactions in electrospun collagen–chitosan complex nanofibers. *Carbohydrate Polymers, 72*(3), 410-418.

Colomines, G., Decaen, P., Lourdin, D., & Leroy, E. (2016). Biofriendly ionic liquids for starch plasticization: a screening approach. *RSC Advances, 6*(93), 90331-90337.

Decaen, P., Rolland-Sabaté, A., Guilois, S., Jury, V., Allanic, N., Colomines, G., et al. (2017). Choline chloride vs choline ionic liquids for starch thermoplasticization. *Carbohydrate Polymers, 177*(Supplement C), 424-432.

Elsabee, M. Z., & Abdou, E. S. (2013). Chitosan based edible films and coatings: A review. *Materials Science and Engineering: C, 33*(4), 1819-1841.

Epure, V., Griffon, M., Pollet, E., & Avérous, L. (2011). Structure and properties of glycerol-plasticized chitosan obtained by mechanical kneading. *Carbohydrate Polymers, 83*(2), 947-952.

Fadzallah, I. A., Majid, S. R., Careem, M. A., & Arof, A. K. (2014). Relaxation process in chitosan–oxalic acid solid polymer electrolytes. *Ionics, 20*(7), 969-975.

Fan, L., Luo, C., Sun, M., Li, X., Lu, F., & Qiu, H. (2012). Preparation of novel magnetic chitosan/graphene oxide composite as effective adsorbents toward methylene blue. *Bioresource Technology, 114*, 703-706.

Fan, L., Luo, C., Sun, M., Li, X., & Qiu, H. (2013). Highly selective adsorption of lead ions by water-dispersible magnetic chitosan/graphene oxide composites. *Colloids and Surfaces B: Biointerfaces, 103*, 523-529.

Gao, C., Pollet, E., & Avérous, L. (2017). Properties of glycerol-plasticized alginate films obtained by thermo-mechanical mixing. *Food Hydrocolloids, 63*, 414-420.

Han, D., Yan, L., Chen, W., & Li, W. (2011). Preparation of chitosan/graphene oxide composite film with enhanced mechanical strength in the wet state. *Carbohydrate Polymers, 83*(2), 653-658.

Iwasaki, N., Yamane, S.-T., Majima, T., Kasahara, Y., Minami, A., Harada, K., et al. (2004). Feasibility of Polysaccharide Hybrid Materials for Scaffolds in Cartilage Tissue Engineering: Evaluation of Chondrocyte Adhesion to Polyion Complex Fibers Prepared from Alginate and Chitosan. *Biomacromolecules, 5*(3), 828-833.

Justin, R., & Chen, B. (2014). Characterisation and drug release performance of biodegradable chitosan–graphene oxide nanocomposites. *Carbohydrate Polymers, 103*, 70-80.

Kavosi, B., Salimi, A., Hallaj, R., & Amani, K. (2014). A highly sensitive prostate-specific antigen immunosensor based on gold nanoparticles/PAMAM dendrimer loaded on MWCNTS/chitosan/ionic liquid nanocomposite. *Biosensors and Bioelectronics, 52*, 20-28.

Khiar, A. S. A., Puteh, R., & Arof, A. K. (2006). Conductivity studies of a chitosan-based polymer electrolyte. *Physica B: Condensed Matter, 373*(1), 23-27.

Kittur, F. S., Vishu Kumar, A. B., & Tharanathan, R. N. (2003). Low molecular weight chitosans—preparation by depolymerization with *Aspergillus niger* pectinase, and characterization. *Carbohydrate Research, 338*(12), 1283-1290.

Lawrie, G., Keen, I., Drew, B., Chandler-Temple, A., Rintoul, L., Fredericks, P., et al. (2007). Interactions between Alginate and Chitosan Biopolymers Characterized Using FTIR and XPS. *Biomacromolecules, 8*(8), 2533-2541.

Lee, K. Y., & Mooney, D. J. (2012). Alginate: Properties and biomedical applications. *Progress in Polymer Science, 37*(1), 106-126.

Leroy, E., Jacquet, P., Coativy, G., Reguerre, A. l., & Lourdin, D. (2012). Compatibilization of starch–zein melt processed blends by an ionic liquid used as plasticizer. *Carbohydrate Polymers, 89*(3), 955-963.

Li, L., Fang, Y., Vreeker, R., Appelqvist, I., & Mendes, E. (2007). Reexamining the Egg-Box Model in Calcium−Alginate Gels with X-ray Diffraction. *Biomacromolecules, 8*(2), 464-468.

Li, Z., Ramay, H. R., Hauch, K. D., Xiao, D., & Zhang, M. (2005). Chitosan–alginate hybrid scaffolds for bone tissue engineering. *Biomaterials, 26*(18), 3919-3928.

Liu, L., Li, C., Bao, C., Jia, Q., Xiao, P., Liu, X., et al. (2012). Preparation and characterization of chitosan/graphene oxide composites for the adsorption of Au(III) and Pd(II). *Talanta, 93*, 350-357.

López, O. V., Ninago, M. D., Lencina, M. M. S., García, M. A., Andreucetti, N. A., Ciolino, A. E., et al. (2015). Thermoplastic starch plasticized with alginate–glycerol mixtures: Melt-processing evaluation and film properties. *Carbohydrate Polymers, 126*(0), 83-90.

Lu, X., Hu, J., Yao, X., Wang, Z., & Li, J. (2006). Composite System Based on Chitosan and Room-Temperature Ionic Liquid: Direct Electrochemistry and Electrocatalysis of Hemoglobin. *Biomacromolecules, 7*(3), 975-980.

Mateescu, M. A., Ispas-Szabo, P., & Assaad, E. (2015). 4 - Chitosan-based polyelectrolyte complexes as pharmaceutical excipients. In M. A. Mateescu, P. Ispas-Szabo, & E. Assaad (Eds.), *Controlled Drug Delivery* (pp. 127-161). Woodhead Publishing.

Mekonnen, T., Mussone, P., Khalil, H., & Bressler, D. (2013). Progress in bio-based plastics and plasticizing modifications. *Journal of Materials Chemistry A*, *1*(43), 13379-13398.

Meng, L., Xie, F., Zhang, B., Wang, D. K., & Yu, L. (2019). Natural Biopolymer Alloys with Superior Mechanical Properties. *ACS Sustainable Chemistry & Engineering*, *7*(2), 2792-2802.

Morris, E. R., Rees, D. A., Thom, D., & Boyd, J. (1978). Chiroptical and stoichiometric evidence of a specific, primary dimerisation process in alginate gelation. *Carbohydrate Research*, *66*(1), 145-154.

Muxika, A., Etxabide, A., Uranga, J., Guerrero, P., & de la Caba, K. (2017). Chitosan as a bioactive polymer: Processing, properties and applications. *International Journal of Biological Macromolecules*, *105*, 1358-1368.

Navaratnam, S., Ramesh, K., Ramesh, S., Sanusi, A., Basirun, W. J., & Arof, A. K. (2015). Transport mechanism studies of chitosan electrolyte systems. *Electrochimica Acta*, *175*, 68-73.

Osman, Z., Ibrahim, Z. A., & Arof, A. K. (2001). Conductivity enhancement due to ion dissociation in plasticized chitosan based polymer electrolytes. *Carbohydrate Polymers*, *44*(2), 167-173.

Pan, Y., Wu, T., Bao, H., & Li, L. (2011). Green fabrication of chitosan films reinforced with parallel aligned graphene oxide. *Carbohydrate Polymers*, *83*(4), 1908-1915.

Papageorgiou, S. K., Kouvelos, E. P., Favvas, E. P., Sapalidis, A. A., Romanos, G. E., & Katsaros, F. K. (2010). Metal–carboxylate interactions in metal–alginate complexes studied with FTIR spectroscopy. *Carbohydrate Research*, *345*(4), 469-473.

Pawlak, A., & Mucha, M. (2003). Thermogravimetric and FTIR studies of chitosan blends. *Thermochimica Acta, 396*(1), 153-166.

Quijada-Garrido, I., Laterza, B., Mazón-Arechederra, J. M., & Barrales-Rienda, J. M. (2006). Characteristic Features of Chitosan/Glycerol Blends Dynamics. *Macromolecular Chemistry and Physics, 207*(19), 1742-1751.

Quijada-Garrido, I., Iglesias-González, V., Mazón-Arechederra, J. M., & Barrales-Rienda, J. M. (2007). The role played by the interactions of small molecules with chitosan and their transition temperatures. Glass-forming liquids: 1,2,3-Propantriol (glycerol). *Carbohydrate Polymers, 68*(1), 173-186.

Ravi Kumar, M. N. V. (2000). A review of chitin and chitosan applications. *Reactive and Functional Polymers, 46*(1), 1-27.

Ren, F., Wang, J., Xie, F., Zan, K., Wang, S., & Wang, S. (2020). Applications of ionic liquids in starch chemistry: a review. *Green Chemistry, 22*(7), 2162-2183.

Rinaudo, M. (2006). Chitin and chitosan: Properties and applications. *Progress in Polymer Science, 31*(7), 603-632.

Sankri, A., Arhaliass, A., Dez, I., Gaumont, A. C., Grohens, Y., Lourdin, D., et al. (2010). Thermoplastic starch plasticized by an ionic liquid. *Carbohydrate Polymers, 82*(2), 256-263.

Shi, R., Zhang, Z., Liu, Q., Han, Y., Zhang, L., Chen, D., et al. (2007). Characterization of citric acid/glycerol co-plasticized thermoplastic starch prepared by melt blending. *Carbohydrate Polymers, 69*(4), 748-755.

Sikorski, P., Mo, F., Skjåk-Bræk, G., & Stokke, B. T. (2007). Evidence for Egg-Box-Compatible Interactions in Calcium−Alginate Gels from Fiber X-ray Diffraction. *Biomacromolecules, 8*(7), 2098-2103.

Šimkovic, I. (2013). Unexplored possibilities of all-polysaccharide composites. *Carbohydrate Polymers, 95*(2), 697-715.

van den Broek, L. A. M., Knoop, R. J. I., Kappen, F. H. J., & Boeriu, C. G. (2015). Chitosan films and blends for packaging material. *Carbohydrate Polymers, 116*, 237-242.

Vieira, M. G. A., da Silva, M. A., dos Santos, L. O., & Beppu, M. M. (2011). Natural-based plasticizers and biopolymer films: A review. *European Polymer Journal, 47*(3), 254-263.

Wang, B., Wan, Y., Zheng, Y., Lee, X., Liu, T., Yu, Z., et al. (2019). Alginate-based composites for environmental applications: a critical review. *Critical Reviews in Environmental Science and Technology, 49*(4), 318-356.

Wang, X., Chi, Y., & Mu, T. (2014). A review on the transport properties of ionic liquids. *Journal of Molecular Liquids, 193*, 262-266.

Wei, C., Zhu, X., Peng, H., Chen, J., Zhang, F., & Zhao, Q. (2019). Facile Preparation of Lignin-Based Underwater Adhesives with Improved Performances. *ACS Sustainable Chemistry & Engineering, 7*(4), 4508-4514.

Wu, G., Ma, X., Fan, L., Gao, Y., Deng, H., & Wang, Y. (2020). Accelerating dermal wound healing and mitigating excessive scar formation using LBL modified nanofibrous mats. *Materials & Design, 185*, 108265.

Xia, L., Long, Y., Li, D., Huang, L., Wang, Y., Dai, F., et al. (2019). LBL deposition of chitosan and silk fibroin on nanofibers for improving physical and biological performance of patches. *International Journal of Biological Macromolecules, 130*, 348-356.

Xie, D. F., Martino, V. P., Sangwan, P., Way, C., Cash, G. A., Pollet, E., et al. (2013). Elaboration and properties of plasticised chitosan-based exfoliated nano-biocomposites. *Polymer, 54*(14), 3654-3662.

Xie, F., Flanagan, B. M., Li, M., Sangwan, P., Truss, R. W., Halley, P. J., et al. (2014). Characteristics of starch-based films plasticised by glycerol and by the ionic liquid 1-ethyl-3-methylimidazolium acetate: A comparative study. *Carbohydrate Polymers, 111*, 841-848.

Xie, F., Flanagan, B. M., Li, M., Truss, R. W., Halley, P. J., Gidley, M. J., et al. (2015). Characteristics of starch-based films with different amylose contents plasticised by 1-ethyl-3-methylimidazolium acetate. *Carbohydrate Polymers, 122*, 160-168.

Yamagata, M., Soeda, K., Ikebe, S., Yamazaki, S., & Ishikawa, M. (2013). Chitosan-based gel electrolyte containing an ionic liquid for high-performance nonaqueous supercapacitors. *Electrochimica Acta, 100*, 275-280.

Yang, J.-S., Xie, Y.-J., & He, W. (2011). Research progress on chemical modification of alginate: A review. *Carbohydrate Polymers, 84*(1), 33-39.

Yang, X., Tu, Y., Li, L., Shang, S., & Tao, X.-m. (2010). Well-Dispersed Chitosan/Graphene Oxide Nanocomposites. *ACS Applied Materials & Interfaces, 2*(6), 1707-1713.

Yu, L., Dean, K., & Li, L. (2006). Polymer blends and composites from renewable resources. *Progress in Polymer Science, 31*(6), 576-602.

Zhang, B., Xie, F., Zhang, T., Chen, L., Li, X., Truss, R. W., et al. (2016). Different characteristic effects of ageing on starch-based films plasticised by 1-ethyl-3-methylimidazolium acetate and by glycerol. *Carbohydrate Polymers, 146*, 67-79.

Zhang, B., Xie, F., Shamshina, J. L., Rogers, R. D., McNally, T., Wang, D. K., et al. (2017). Facile Preparation of Starch-Based Electroconductive Films with Ionic Liquid. *ACS Sustainable Chemistry & Engineering, 5*(6), 5457-5467.